

A TWO-ZONE MODEL FOR BLAZAR EMISSION: IMPLICATIONS FOR TXS 0506+056 AND THE NEUTRINO EVENT ICECUBE-170922A

RUI XUE^{1, 7}, RUO-YU LIU², MARIA PETROPOULOU³, FOTEINI OIKONOMOU⁴, ZE-RUI WANG^{1, 7}, KAI WANG^{5, 6} AND XIANG-YU WANG^{1, 7}

¹School of Astronomy and Space Science, Nanjing University, Nanjing 0110093, China

²Deutsches Elektronen Synchrotron (DESY), Platanenallee 6, D-15738 Zeuthen, Germany

³Department of Astrophysical Sciences, Princeton University, 4 Ivy Lane, Princeton, NJ 08544, USA

⁴European Southern Observatory, Karl-Schwarzschild-Str 2, D-85748 Garching bei Munchen, Germany

⁵Department of Astronomy, School of Physics, Peking University, Beijing 100871, China

⁶Kavli Institute for Astronomy and Astrophysics, Peking University, Beijing 100871, China

⁷Key laboratory of Modern Astronomy and Astrophysics (Nanjing University), Ministry of Education, Nanjing 210023, People's Republic of China

ABSTRACT

A high-energy muon neutrino event, IceCube-170922A, was recently discovered in both spatial and temporal coincidence with a gamma-ray flare of the blazar TXS 0506+056. It has been shown, with standard one-zone models, that neutrinos can be produced in the blazar jet via hadronic interactions, but with a flux which is mostly limited by the X-ray data. In this work, we explore the neutrino production from TXS 0506+056 by invoking two physically distinct emission zones in the jet, separated by the broad line region (BLR). Using the Doppler-boosted radiation of the BLR as the target photon field, the inner zone accounts for the neutrino and gamma-ray emission via $p\gamma$ interactions and inverse Compton scattering respectively, while the outer zone produces the optical and X-ray emission via synchrotron and synchrotron self-Compton processes. The different conditions of the two zones allow us to suppress the X-ray emission from the electromagnetic cascade, and set a much higher upper limit on the muon neutrino flux (i.e., $\sim 10^{-11}$ erg cm⁻²s⁻¹) than in one-zone models. We compare, in detail, our scenario with one-zone models discussed in the literature, and argue that differentiating between such scenarios will become possible with next generation neutrino telescopes, such as IceCube-Gen2.

Keywords: neutrinos — radiation mechanisms: non-thermal — BL Lacertae objects: individual (TXS 0506+056)

1. INTRODUCTION

Blazars are a special class of active galactic nuclei (AGN), with relativistic jets closely aligned to our line of sight (Urry & Padovani 1995). Being some of the most powerful persistent sources of electromagnetic (EM) radiation in the Universe, with typical bolometric luminosities of 10^{43} - 10^{48} erg s⁻¹, blazars have been widely considered as candidate sources for high-energy cosmic rays and neutrinos (e.g., Mannheim et al. 1992; Atoyan, & Dermer 2001; Murase et al. 2014; Petropoulou et al. 2015; Padovani et al. 2016; Paladino et al. 2019).

On September 22, 2017, a 290 TeV muon neutrino, IceCube-170922A, triggered the IceCube extremely-high-energy (EHE) online event filter (IceCube Collaboration et al. 2018). For the first time, a high-energy neutrino was detected in temporal and spatial coincidence with a multi-wavelength flare from

a known blazar (TXS 0506+056), with a significance of $\sim 3\sigma$. This event has been extensively studied in the framework of conventional one-zone leptonic models with photohadronic ($p\gamma$) interactions (Ansoldi et al. 2018; Keivani et al. 2018; Gao et al. 2019; Cerruti et al. 2019). In these models, the multi-wavelength spectral energy distribution (SED) of the flare is explained by the synchrotron radiation and Compton processes of relativistic electrons injected into a localized radiation zone inside the jet (the so-called emitting blob), while neutrinos are produced via the $p\gamma$ interaction between relativistic protons and synchrotron photons. Electron-positrons pairs (henceforth, secondary pairs) are also produced by the $p\gamma$ interactions and Bethe-Heitler (BH) pair production processes of relativistic protons. Extremely high-energy photons, produced either by the decay of neutral pions or by the synchrotron emission of secondary pairs, are absorbed in the soft (syn-

chrotron) radiation field via $\gamma\gamma$ pair production (e.g., Mannheim & Biermann 1992), thus transferring their energy to relatively lower-energy photons (e.g., from X-rays to MeV and TeV γ -rays) through an EM cascade in the blob (e.g., Petropoulou & Mastichiadis 2015). The (quasi-)simultaneous X-ray observations from *Swift* and *NuSTAR* provide a stringent constraint on the cascade emission (Keivani et al. 2018; Murase et al. 2018). Since both the EM cascade emission and the neutrino emission originate from the $p\gamma$ interactions on the same target photon field, the X-ray data can also constrain the neutrino flux, yielding a detection rate $< 0.03 \text{ yr}^{-1}$ (Keivani et al. 2018; Gao et al. 2019) after convolving with the effective area of the IceCube EHE track-event alert system¹ (IceCube Collaboration et al. 2018).

Such a low detection rate translates to a probability of $\lesssim 1\%$ for IC-170922A to have triggered IceCube’s alert system, assuming that the blazar flare lasted only several months. While it may be possible to explain the detection of one neutrino from TXS 0506+056 as a consequence of the Eddington bias (Strotjohann et al. 2019), it is worth investigating if a higher neutrino flux and hence a more comfortable detection probability of the event can be obtained in other theoretical scenarios. Liu et al. (2019) proposed that a high neutrino flux can be obtained, if a second emitting zone forms inside the broad-line region (BLR) of the blazar, in addition to the emitting blob considered in the conventional one-zone model which accounts for the EM emission of the blazar. In that scenario, accelerated protons interact with BLR clouds that enter the jet and produce neutrinos efficiently via proton–proton (pp) inelastic collisions, with the resulting X-ray flux still being consistent with the observations. The idea of two emitting zones and their potential to improve the predicted neutrino detection rate has also been discussed by Murase et al. (2018) in the context of the neutral beam model (Atoyan & Dermer 2003; Dermer et al. 2012) and by Zhang et al. (2019).

Generally speaking, two-zone scenarios invoke a second emitting region with additional free parameters, thus introducing more uncertainties to the model. However, the presence of multiple emission sites in blazar jets is physically plausible. For example, substructures, such as multiple bright knots and hot spots, have been observed along the jets of radio galaxies (see e.g., Harris & Krawczynski 2006, for a review),

which are thought to be the off-axis counterparts of blazars (Urry & Padovani 1995; Abdo et al. 2010), implying that particle acceleration and emission can take place at different parts of a jet at the same time. These features have been discovered in jets of different lengths, spanning from kiloparsec to Megaparsec scales. Here, we speculate that multiple radiation zones may also exist in the inner (sub-)parsec scale jets of blazars. The recent discovery of significant offsets between the optical core and the radio core pinpointed respectively with Gaia and VLBI in many blazars (Plavin et al. 2019) may lend support to our assumption. There are also indications of multiple emitting zones in individual blazars (e.g., Nalewajko et al. 2012; Prince et al. 2019). Even if the intrinsic properties of different emitting zones, such as their Doppler factor and size, are similar to each other, their external environment may be different. For example, if the emitting region is located within the BLR, the latter provides an extra target photon field for the inverse Compton scattering of electrons and for the photohadronic ($p\gamma$) interactions of protons. It may also provide the dense clouds required by the pp collision mechanism (Sahakyan 2018; Liu et al. 2019). Therefore, the resulting radiation from an emitting zone inside (close to) the BLR can be very different from that outside (far away from) the BLR, when considering the properties of the external environment.

TXS 0506+056 is classified as a BL Lac object based on the low equivalent width (EW) of three very weak emission lines (Stickel et al. 1991; Stocke et al. 1991) identified in its optical spectrum (Paiano et al. 2018). However, this should not be interpreted as evidence for the lack of a BLR, since the radiation of the latter could be overwhelmed by the intense non-thermal emission from the jet (Georganopoulos & Marscher 1998; Giommi et al. 2012, 2013). Interestingly, a recent paper by Padovani et al. (2019) pointed out that TXS 0506+056 is in fact a masquerading BL Lac object, with a hidden BLR with luminosity $\approx 5 \times 10^{43} \text{ erg s}^{-1}$ and a standard accretion disk.

Motivated by both theoretical and observational perspectives, we set to explore the neutrino emission from TXS 0506+056 in the framework of a two-zone $p\gamma$ model that takes into account the existence of the BLR. Our main goals are to compute the maximum neutrino flux predicted by the model, while fitting the SED with two radiation zones, and to understand the fundamental differences with the standard one-zone models. The rest of this paper is structured as follows. In Section 2 we present the general description of the two-zone $p\gamma$ model and apply it to the 2017 observations of TXS 0506+056. In Section 3 we show the differences between the two-zone $p\gamma$ model and the one-zone model, and explain the reasons why the former model can result in higher

¹ In some literature, the neutrino detection rate is calculated with the normal IceCube effective area for muon neutrino which is about 10 times higher than that of the EHE through-going muon-track event filter, resulting in a 10 times higher detection rate than the one presented here.

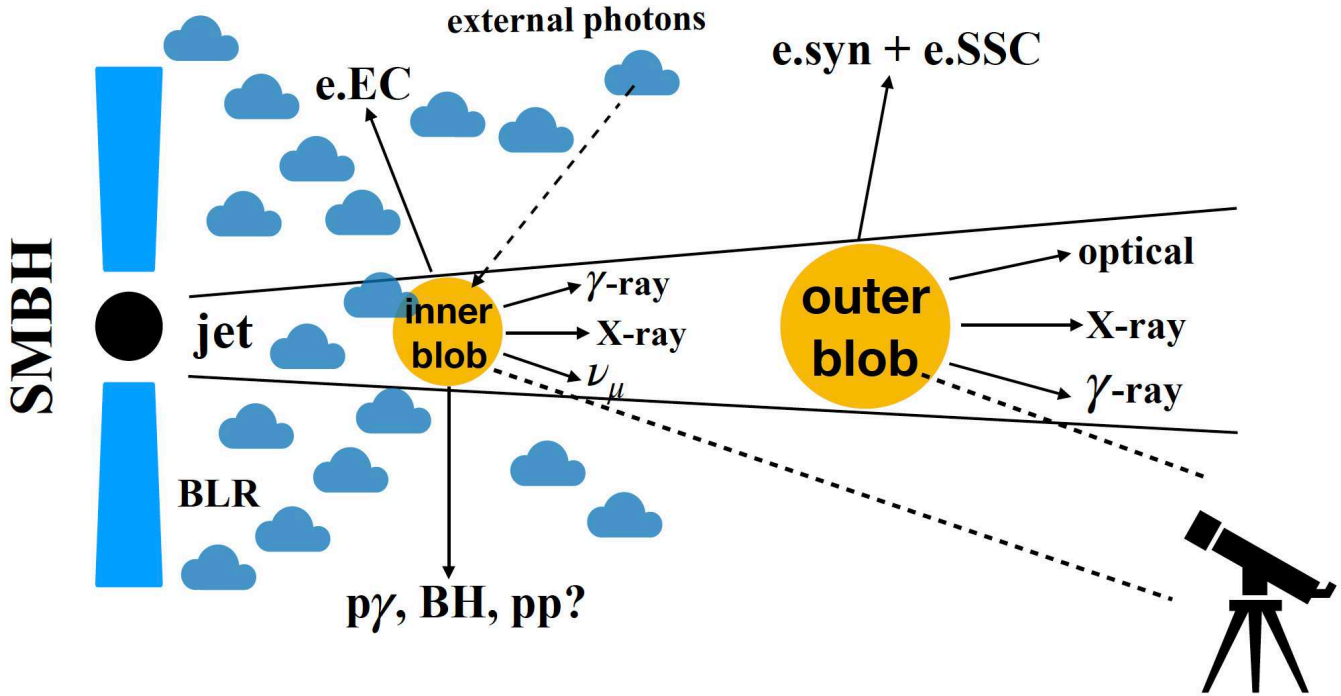


Figure 1. A schematic illustration (not to scale) of the two-zone photohadronic ($p\gamma$) model. The outer blob is far away from the BLR and the inner blob is close or inside the BLR. In the presence of the external radiation field provided by the BLR, the inner blob is assumed to be an efficient γ -ray (via external Compton emission of electrons, denoted here as e.EC) and neutrino emitter due to the $p\gamma$ process or possibly the pp process. The emission of the cascade initiated by electromagnetic secondaries produced in $p\gamma$, Bethe-Heitler or pp processes can emerge in X-rays and gamma rays. The low-energy radiation is probably suppressed due to the dominant Compton cooling of electrons. The observed low-energy radiation arises from the synchrotron emission of electrons (e.syn) from the outer blob where the BLR radiation is negligible. The outer blob may also produce hard X-ray and γ -ray photons via the SSC process (e.SSC) of accelerated electrons.

maximal neutrino fluxes. In Section 4 we discuss our results, while paying particular attention to potential methods of differentiating among models in the future. Our conclusions are presented in Section 5. Throughout the paper, we adopt the Λ CDM cosmology with $H_0 = 70 \text{ km s}^{-1} \text{ Mpc}^{-1}$, $\Omega_m = 0.3$, $\Omega_\Lambda = 0.7$.

2. MODEL DESCRIPTION AND APPLICATION

Although there might be multiple emitting zones in the blazar jet, here we consider the simplest multi-zone scenario which consists of two regions, one far away from the BLR (the outer blob) and another one close to or inside the BLR (the inner blob). In the presence of the external radiation field provided by the BLR, the inner blob is assumed to be an efficient gamma-ray and neutrino emitter, while the low-energy (i.e., from infrared to soft X-ray) radiation of synchrotron origin is likely suppressed. In our scenario, the observed low-energy radiation most likely arises from the outer blob where the BLR radiation is negligible. The outer blob may also produce hard X-ray and gamma-ray photons via the SSC process of electrons. A sketch of our model is shown in Fig. 1.

A detailed description of the model can be found in the

following subsections. Henceforth, physical quantities with the superscript “AGN” are measured in the AGN frame, whereas quantities without the superscript are measured in the jet’s comoving frame, unless otherwise specified.

2.1. The leptonic emission from the outer blob

Relativistic electrons are assumed to be injected in the outer blob with a smooth broken power-law energy distribution (Ghisellini et al. 2010) at a constant rate given by:

$$Q_e(\gamma_e) = Q_{e,0} \gamma_e^{-n_{e,1}} \left[1 + \left(\frac{\gamma_e}{\gamma_{e,b}} \right)^{(n_{e,2} - n_{e,1})} \right]^{-1}, \quad (1)$$

for $\gamma_{e,\min} < \gamma_e < \gamma_{e,\max}$,

where $\gamma_{e,\min}$, $\gamma_{e,b}$ and $\gamma_{e,\max}$ are the minimum, break and maximum electron Lorentz factors, $n_{e,1}$ and $n_{e,2}$ are the power-law indices below and above $\gamma_{e,b}$, respectively, and $Q_{e,0}$ is a normalization constant. This is determined by $\int Q_e \gamma_e m_e c^2 d\gamma_e = 3 L_{e,\text{inj}} / (4\pi R_{\text{out}}^3)$, where $L_{e,\text{inj}}$ is the electron injection luminosity and R_{out} is the radius of the outer blob, m_e is the electron rest mass, and c is the speed of light. The steady-state electron density

distribution can be then written as:

$$N_e(\gamma_e) \approx Q_e(\gamma_e)t_e, \quad (2)$$

where $t_e = \min\{t_{\text{cool}}, t_{\text{esc, out}}\}$ with $t_{\text{esc, out}} = R_{\text{out}}/c$ being the particle escape timescale of the outer blob (in the ballistic propagation limit) and $t_{\text{cool}} = 3m_e c / (4(U_B + \kappa_{\text{KN}} U_{\text{ph}}) \sigma_T \gamma_e)$ being the electron radiative cooling timescale. Here, $U_B = B^2/8\pi$ is the energy density of the magnetic field, U_{ph} is the energy density of the soft photons, σ_T is the Thomson scattering cross section, and κ_{KN} is a numerical factor accounting for Klein-Nishina effects (Moderski et al. 2005). Using the steady-state electron distribution $N_e(\gamma_e)$, we can then compute the synchrotron and synchrotron self-Compton (SSC) emissions (Katarzyński et al. 2001). Since we assume that the outer blob is far away from the BLR, the external Compton (EC) emission is not considered here.

Relativistic protons are also assumed to be injected in the outer blob with a power-law energy distribution and at a constant rate:

$$Q_p(\gamma_p) = Q_{p,0} \gamma_p^{-n_p}, \quad \gamma_{p,\text{min}} < \gamma_p < \gamma_{p,\text{max}}, \quad (3)$$

where n_p is the power-law index, $\gamma_{p,\text{min}}$ and $\gamma_{p,\text{max}}$ are the minimum and maximum proton Lorentz factors, respectively, and $Q_{p,0}$ is a normalization constant. This is determined by $\int Q_p \gamma_p m_p c^2 d\gamma_p = 3 L_{p,\text{inj}} / (4\pi R_{\text{out}}^3)$, where $L_{p,\text{inj}}$ is the proton injection luminosity and m_p is the proton rest mass. Similar to the electrons, the steady-state proton distribution can be written as:

$$N_p(\gamma_p) \approx Q_p(\gamma_p)t_p, \quad (4)$$

where $t_p = \min\{t_{p\gamma}, t_{\text{BH}}, t_{\text{esc, out}}, t_{p,\text{syn}}\}$. More specifically, $t_{p\gamma} = [cn_{\text{soft}} < \sigma_{p\gamma} \kappa_{p\gamma} >]^{-1}$ is the $p\gamma$ energy loss timescale, where n_{soft} is the number density of the soft photons and $< \sigma_{p\gamma} \kappa_{p\gamma} > \simeq 10^{-28} \text{cm}^2$ is the inelasticity-weighted $p\gamma$ interaction cross-section. $t_{\text{BH}} = [cn_{\text{soft}} < \sigma_{\text{BH}} \kappa_{\text{BH}} >]^{-1}$ is the BH pair-production cooling timescale, where σ_{BH} and κ_{BH} are, respectively, the cross section and inelasticity for the BH pair production process (Chodorowski et al. 1992). Finally, $t_{p,\text{syn}} = 6\pi m_e c^2 / (c\sigma_T B^2 \gamma_p) (m_p/m_e)^3$ is the proton-synchrotron cooling timescale.

In the outer blob, the only target radiation field for the $p\gamma$ process and the BH process is the synchrotron emission of primary electrons, which is inefficient for protons of energy < 10 PeV (see Fig. 2). Thus, the hadronic emission of the outer blob can be neglected unless a highly super-Eddington proton kinetic luminosity is assumed.

2.2. The leptonic and hadronic emission from the inner blob

We assume that electrons and protons are injected into the inner blob at the same rate as in the outer blob

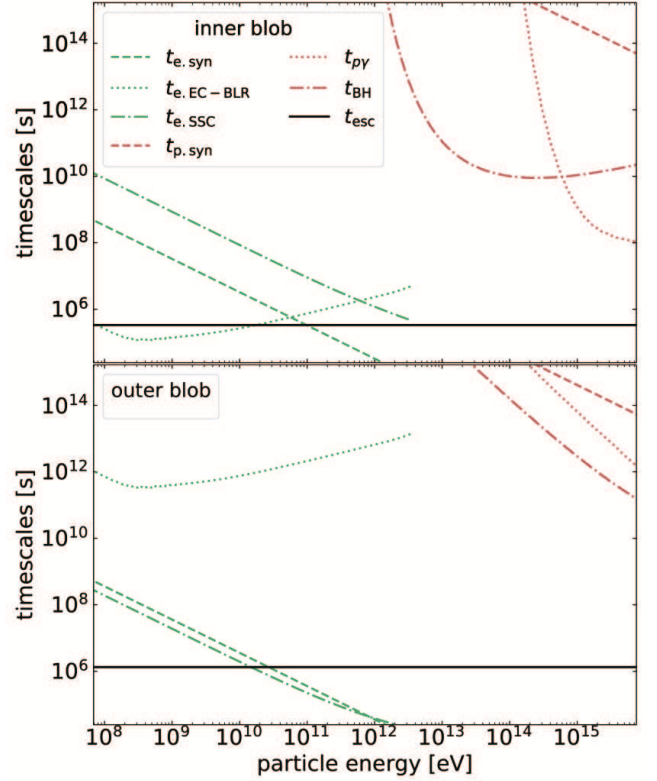


Figure 2. Timescales of various cooling processes for electrons (green curves) and protons (red curves) in the inner blob (upper panel) and outer blob (lower panel) as a function of the particle energy. Both the particle energy and timescale are measured in the jet's comoving frame. Parameters are the same in those in Fig. 3. The black horizontal lines denote the escape timescale of particles in the ballistic propagation limit. The meaning of all curves is explained in the inset legend.

(see Eqs. (1) and (3)). The steady-state energy spectra of primary electrons and protons are given by Eqs. (2) and (4), respectively, with the only difference that U_{ph} and n_{soft} are now dominated by the BLR photons due to the blob location in the jet (see also Fig. 1).

The energy density of BLR radiation in the jet comoving frame (u_{BLR}) as a function of the distance along the jet, $r_{\text{in}}^{\text{AGN}}$, can be approximately written as (Hayashida et al. 2012):

$$u_{\text{BLR}} \approx \frac{\Gamma^2 L_{\text{BLR}}^{\text{AGN}}}{4\pi (r_{\text{BLR}}^{\text{AGN}})^2 c [1 + (r_{\text{in}}^{\text{AGN}}/r_{\text{BLR}}^{\text{AGN}})^3]}, \quad (5)$$

where Γ is the bulk Lorentz factor of the jet². $L_{\text{BLR}}^{\text{AGN}}$ is the BLR luminosity in AGN frame and $r_{\text{BLR}}^{\text{AGN}} = 0.1(L_{\text{BLR}}^{\text{AGN}}/10^{45} \text{erg s}^{-1})^{1/2}$ pc is the characteristic radius of the BLR in the AGN frame. The energy spectrum of the BLR radiation is taken to be that of black

² For simplicity, we assume the Doppler factor $\delta_D \approx \Gamma$ for a relativistic jet close to the line of sight in blazars with a viewing angle of $\theta \lesssim 1/\Gamma$ hereafter.

body with a peak at $\approx 3.93k_B T\Gamma/h \approx 2 \times 10^{15}\Gamma$ Hz (Tavecchio & Ghisellini 2008). The inner blob is assumed to be located close to or inside the BLR, i.e., $r_{\text{in}}^{\text{AGN}} \sim r_{\text{BLR}}^{\text{AGN}}$.

We neglect the radiation of protons that leave the inner blob, as they will cool adiabatically on a timescale $\sim r_{\text{BLR}}^{\text{AGN}}/(c\delta_D) \sim 10^6(r_{\text{BLR}}^{\text{AGN}}/10^{17}\text{cm})(\delta_D/20)^{-1}$ s in the jet's comoving frame. This is generally much shorter than the photohadronic energy loss timescales (see Fig. 2), especially if one considers that the BLR radiation density, which dominates the proton photohadronic losses, decreases quickly at larger distances (see Eq. 5).

Using the steady-state proton distribution $N_p(\gamma_p)$ and following Kelner & Aharonian (2008), we compute the differential spectra of: γ -ray photons from neutral pion decays, electrons/positrons, and neutrinos produced in the photopion production and BH pair-production processes. The spectrum of secondary electrons generated in the pair cascade is evaluated using a semi-analytical method developed by Böttcher et al. (2013); Wang et al. (2018) (see also Yan & Zhang 2015). The synchrotron, SSC and EC emission of the pair cascade is also calculated.

Lastly, any very high energy (VHE) γ -ray photons that escape from the inner or the outer blobs will be absorbed by the extragalactic background light (EBL). To account for this attenuation in the GeV-TeV band, we use the EBL model of Domínguez et al. (2011).

2.3. Parameters constraints

To reduce the number of free parameters as much as possible, we assume that the two regions have the same electron luminosity ($L_{e,\text{inj}}$), the same proton luminosity ($L_{p,\text{inj}}$), as well as the spectral shape of injected particles. They also have the same magnetic field B , and they move with the same Doppler factor δ_D . With such a setup³, our two-zone $p\gamma$ model has sixteen free parameters: six for the two radiation zones (δ_D , B , R_{out} , R_{in} , $r_{\text{in}}^{\text{AGN}}$ and $L_{\text{BLR}}^{\text{AGN}}$), six for the injected primary relativistic electrons in the two blobs ($L_{e,\text{inj}}$, $n_{e,1}$, $n_{e,2}$, $\gamma_{e,\text{min}}$, $\gamma_{e,b}$ and $\gamma_{e,\text{max}}$) and four for the injected relativistic protons in the inner blob ($L_{p,\text{inj}}^{\text{AGN}}$, n_p , $\gamma_{p,\text{min}}$ and $\gamma_{p,\text{max}}$). Our strategy for reducing further the number of free parameters is described below.

1. We set $L_{\text{BLR}}^{\text{AGN}} = 5 \times 10^{43}\text{erg s}^{-1}$, as estimated by Padovani et al. (2019). The characteristic size of the BLR is then $r_{\text{BLR}}^{\text{AGN}} = 0.02$ pc.
2. In leptonic models, the minimum electron Lorentz factor $\gamma_{e,\text{min}}$ is usually constrained by the hard

X-ray data, since this is the energy band where the low-energy tail of the SSC emission emerges (Celotti & Ghisellini 2008; Madejski et al. 2016). However, when hadronic interactions are considered, the synchrotron radiation of secondary electrons generated in the pair cascade will also contribute to the hard X-ray band. Therefore, $\gamma_{e,\text{min}}$ cannot be constrained in a straightforward manner by the SED fitting. In our calculations, we therefore adopt a typical value of $\gamma_{e,\text{min}} = 50$.

3. We set the maximum electron Lorentz factor $\gamma_{e,\text{max}} = 10^7$, since it does not have a major impact on our model results.
4. We set the power-law index of the proton spectrum at injection to be $n_p = 2$.
5. We adopt $\gamma_{p,\text{min}} = 1$ for the minimum proton Lorentz factor. Its exact value will not affect our fitting results, but only the energetic requirements.
6. Generally, $\gamma_{p,\text{max}}$ can be obtained by equating the acceleration timescale to the minimum of the energy loss and escape timescales. The acceleration timescale can be evaluated by (Protheroe & Clay 2004; Rieger et al. 2007)

$$t_{\text{acc}} \simeq \frac{\alpha r_L}{c} \simeq \frac{\alpha \gamma_p m_p c}{eB}, \quad (6)$$

where r_L is the Larmor radius of the relativistic proton and $\alpha(> 1)$ is a model parameter depending on the detailed mechanism. Since the detected neutrino energy is most likely $\lesssim \text{PeV}$, the maximum proton energy in the jet's comoving frame should be larger than $\sim 1(\delta_D/20)^{-1}$ PeV. Using $\alpha = 50$ (Lagage & Cesarsky 1983) and assuming that the acceleration is hindered by physical escape from the system, the maximum proton Lorentz factor is:

$$\gamma_{p,\text{max}} = \frac{eBR_{\text{in}}}{\alpha m_p c^2} \simeq 6.4 \times 10^7 \left(\frac{\alpha}{50}\right)^{-1} \left(\frac{B}{1\text{G}}\right) \left(\frac{R_{\text{in}}}{10^{16}\text{cm}}\right) \quad (7)$$

which satisfies the condition to produce PeV neutrinos.

7. Assuming that the SMBH mass of TXS 0506+056 is $10^9 M_\odot$, the Eddington luminosity of the SMBH is $L_{\text{Edd}} = 1.3 \times 10^{47}\text{erg/s}$. We set the kinetic proton luminosity for both blobs to be the Eddington luminosity, or an injection luminosity $L_{p,\text{inj}} \simeq L_{\text{Edd}}/\delta_D^2$ in the blob.

Finally, the number of free parameters is reduced to nine, namely δ_D , B , R_{out} , R_{in} , $L_{e,\text{inj}}$, $r_{\text{in}}^{\text{AGN}}$, $n_{e,1}$, $n_{e,2}$ and $\gamma_{e,b}$.

³ We discuss how a different choice of the model parameters for the two blobs would affect our results in Appendix A.

Table 1. Parameters for SED fitting with the two-zone $p\gamma$ model. We assume a large distance of the outer blob to the SMBH (e.g., $\sim 10 \text{ pc} \gg r_{\text{BLR}}^{\text{AGN}}$) so that it is not influenced by the BLR radiation.

Free Parameters	δ_{D}	B	R_{out}	R_{in}	$L_{\text{e},\text{inj}}$	$r_{\text{in}}^{\text{AGN}}$	$n_{\text{e},1}$	$n_{\text{e},2}$	$\gamma_{\text{e},\text{b}}$
		[G]	[cm]	[cm]	[erg/s]	[pc]			
Values	26.5	0.11	4×10^{16}	1×10^{16}	2×10^{42}	0.05	1.4	4	8.1×10^3
Fixed/Derived parameters	$L_{\text{BLR}}^{\text{AGN}}$	$L_{\text{p},\text{inj}}$	$\gamma_{\text{e},\text{min}}$	$\gamma_{\text{e},\text{max}}$	n_{p}	$\gamma_{\text{p},\text{min}}$	$\gamma_{\text{p},\text{max}}$	$L_{\text{e},\text{in}}^{\text{k}}$	$L_{\text{p},\text{in}}^{\text{k}}$
	[erg/s]	[erg/s]						[erg/s]	[erg/s]
Values	5×10^{43}	1.97×10^{44}	50	10^7	2	1	7.04×10^6	3.83×10^{43}	1.3×10^{47}

NOTE—The kinetic luminosity in relativistic electrons $L_{\text{e},\text{in}}^{\text{k}}$ and in relativistic protons $L_{\text{p},\text{in}}^{\text{k}}$ in the inner blob are calculated as $L_{\text{e},\text{in}}^{\text{k}} \simeq \pi R_{\text{in}}^2 \delta_{\text{D}}^2 m_e c^3 \int \gamma_e N_e(\gamma_e) d\gamma_e$ and $L_{\text{p},\text{in}}^{\text{k}} \simeq \pi R_{\text{in}}^2 \delta_{\text{D}}^2 m_p c^3 \int \gamma_p N_p(\gamma_p) d\gamma_p \simeq (3/4) \delta_{\text{D}}^2 L_{\text{p},\text{inj}}$. Due to the strong cooling of electrons, there is no simple relation between electrons’ injection luminosity and its kinetic luminosity.

2.4. Application to TXS 0506+056 and IC-170922A

We apply the two-zone $p\gamma$ model to the 2017 multi-messenger observations of TXS 0506+056. Our model-predicted SED and neutrino spectrum for the parameters shown in Table 1 are presented in Fig. 3. The low-energy bump in the SED is explained by the synchrotron emission of primary electrons in the outer blob, while the hard X-ray flux and part of the GeV flux is attributed to their SSC emission. The primary electrons in the inner blob cool very fast in the Doppler-boosted BLR radiation field. The synchrotron radiation of these electrons is suppressed, as they radiate away their energy mainly through the EC process⁴ (see also Fig. 2), which makes an important contribution to the *Fermi*-LAT γ -ray flux. In addition, the emission from the pair cascade mainly accounts for the TeV emission. We note that this is not a unique representation of the SED, as different parameter sets can lead to equally good descriptions of the blazar spectrum. We refer readers to Appendix A for a detailed discussion on this topic.

By convolving the neutrino flux shown in Fig. 3 with the effective area of IceCube’s EHE event alert system (IceCube Collaboration et al. 2018), we derive the predicted neutrino detection rate. This is $\sim 0.3 \text{ yr}^{-1}$ in the range of 0.2 – 7.5 PeV, which is one order of magnitude higher than the one predicted by standard one-zone models (Keivani et al. 2018; Cerruti et al. 2019; Gao et al. 2019).

To compute the number of predicted muon neutrinos from TXS 0506+056, one needs to know the duration of neutrino production in addition to the predicted production rate. Since only one neutrino event (IC-170922A) was detected during the \sim six-month long γ -ray flare of TXS 0506+056 in 2017, the neutrino emission period cannot be securely determined from the observations. From the theoretical point of view, in the two-zone $p\gamma$

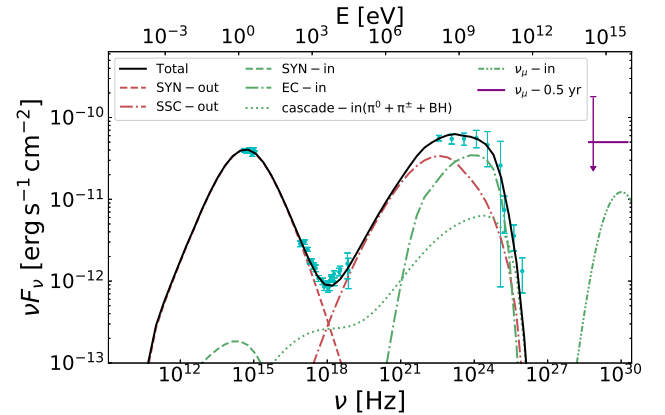


Figure 3. The (quasi-)simultaneous SED of TXS 0506+056 within two weeks of the detection of IC-170922A (on MJD 58019). Data (colored symbols) are taken from IceCube Collaboration et al. (2018). The dashed red and dotted-dashed red curves represent the synchrotron and SSC emission from primary electrons in the outer blob, respectively. The dotted green and dot-dashed green curve represents the synchrotron emission and EC emission of primary electrons in the inner blob respectively, while the dotted green curve represents the emission from pair cascades in the inner blob. The double dotted-dashed green curve shows the muon neutrino energy spectrum. The SSC emission of primary electrons in the inner blob is too low to be visible in this figure. The solid black curve is the total emission from the outer blob and II. The representative solid purple lines show the required $\nu_{\mu} + \bar{\nu}_{\mu}$ neutrino flux to produce one EHE alert event like IC-170922A over a period of half year, assuming a neutrino spectrum of E^{-2} .

model considered here, the period of γ -ray flaring activity and enhanced neutrino production can, in principle, be different. The reason is that the γ -ray emission may be explained solely by the radiative processes of primary electrons in the outer blob, while the neutrino emission is mainly produced in the inner blob via $p\gamma$ interactions of relativistic protons with the BLR photons. If the inner blob is moving relativistically towards the observer, the neutrino emission at the predicted rate of $\sim 0.3 \text{ yr}^{-1}$ would only last for a time equal to the maximum of the following two characteristic timescales: the light-crossing timescale of the inner blob (i.e., $\sim R_{\text{in}}/\delta_{\text{D}}c$) and

⁴ The energy density of BLR at $r_{\text{in}}^{\text{AGN}}$ is $\sim 1.6 \text{ erg cm}^{-3}$, which is much higher than the magnetic energy density, i.e. $\sim 0.0004 \text{ erg cm}^{-3}$.

the time needed for the inner blob to travel beyond the BLR (as seen in the observer’s frame), i.e., a few times $r_{\text{in}}^{\text{AGN}}/\delta_{\text{D}}^2 c$, which are both less than one day. This short duration would result in a very low detection probability in spite of the high neutrino production rate. In order to obtain higher detection probabilities within our model, the neutrino production rate of $\sim 0.3 \text{ yr}^{-1}$ should be sustained for several months. This might be realized if multiple blobs, like the inner blob, would form close to or inside the BLR as a result of continuous dissipation for a period of several months. Alternatively, the inner blob could be associated with dissipation happening at a quasi-stationary feature (such as re-collimation shock, e.g., [Fromm et al. 2011](#)) close to or inside the BLR, lasting the same amount of time.

3. COMPARISON WITH ONE-ZONE MODELS

The main difference between the two-zone $p\gamma$ model from the standard one-zone models is that the emission accounting for the low-energy bump of the blazar SED originates from a different region than the one where neutrinos are produced. This is the key to overcome the constraint from the X-ray flux on the cascade emission and hence increase the maximal predicted neutrino flux. To further explain this point, let us first review briefly the reason why one-zone $p\gamma$ models always result in lower neutrino fluxes.

3.1. One-Zone SSC Model

For a typical Doppler factor of the blazar jet $\delta_{\text{D}} \sim 10$, PeV neutrinos are produced through the $p\gamma$ process most efficiently on soft X-ray photons (as viewed in the jet’s comoving frame). In the one-zone SSC model, the target photon field is the synchrotron radiation of primary electrons, which accounts for the low-energy bump in the SED of TXS 0506+056. The comoving synchrotron spectrum peaks in the infrared, thus resulting in a very low number density in the X-ray band. Consequently, the PeV neutrino production efficiency is low, as it has also been pointed out in previous studies. There are in principle two potential ways of overcoming this problem and of increasing the neutrino flux.

The first one is to increase the $p\gamma$ interaction efficiency $f_{p\gamma}$. This can be achieved by increasing the number density of the synchrotron radiation in the comoving frame by employing a relatively low Doppler factor δ_{D} and/or small blob size R . At the same time, however, the opacity for $\gamma\gamma$ absorption of high-energy gamma rays by the synchrotron photons will also increase by the same factor (i.e., $\tau_{\gamma\gamma} \propto \delta_{\text{D}}^{-4} R^{-1}$, [Dermer et al. 2012](#); [Petropoulou et al. 2017](#); [Xue et al. 2019](#)). Note that the synchrotron radiation provides abundant infrared photons which efficiently absorb co-produced gamma-ray photons with sub-PeV/PeV en-

ergy and deposit their energy via the pair cascade into the X-ray band ([Petropoulou & Mastichiadis 2015](#); [Murase et al. 2016](#)). Although the neutrino luminosity is $L_{\nu} \propto f_{p\gamma} L_{\text{p}}$, the X-ray luminosity from the cascade is $L_{\text{X}} \propto \tau_{\gamma\gamma} f_{p\gamma} L_{\text{p}} \propto f_{p\gamma}^2 L_{\text{p}}$. Thus, if one attempts to increase $f_{p\gamma}$ to produce a higher neutrino flux, the X-ray flux of the EM cascade will unavoidably increase as $f_{p\gamma}^2$. The *Swift*/XRT and *NuSTAR* X-ray observations of TXS 0506+056 are placing strong constraints on $f_{p\gamma}$ ([Keivani et al. 2018](#); [Murase et al. 2018](#); [Gao et al. 2019](#)).

Alternatively, one can employ a high proton luminosity to counterbalance the low neutrino production efficiency. Given that $L_{\text{X}} \propto f_{p\gamma}^2 L_{\text{p}}$, a high neutrino flux can be obtained simultaneously with a low X-ray flux from cascade by invoking a sufficiently small $f_{p\gamma}$ and a sufficiently large L_{p} . However, the required proton luminosity would be highly super-Eddington (see also [Petropoulou et al. 2015](#)).

Practically speaking, the fitting of the high-energy bump of the SED with the SSC emission of primary electrons requires a proper energy density of the synchrotron radiation (e.g., [Mastichiadis & Kirk 1997](#)). Thus, the neutrino production efficiency is more or less fixed. The neutrino detection rate predicted by previous studies of the 2017 multi-messenger flare of TXS 0505+056 within the one-zone SSC model, when the pair cascade emission saturates the X-ray data, is $\sim 0.01 - 0.03 \text{ yr}^{-1}$. Still, the required proton luminosity exceeds the Eddington limit by several tens to a few hundred times (assuming a black hole mass of $M_{\text{BH}} = 10^9 M_{\odot}$).

3.2. One-Zone EC model

In the one-zone EC model, external photons such as photons from the BLR (e.g., [Atoyan, & Dermer 2001](#); [Dermer et al. 2014](#); [Murase et al. 2014](#)), the accretion disk or accretion flow (e.g., [Stecker et al. 1991](#); [Bednarek & Protheroe 1999](#); [Alvarez-Muñiz, & Mészáros 2004](#); [Kimura et al. 2015](#); [Righi et al. 2019](#)), or the sheath region of the jet (e.g., [Tavecchio et al. 2014](#); [Tavecchio, & Ghisellini 2015](#)), can significantly enhance the $p\gamma$ interaction efficiency and the neutrino flux, and thus may reduce the required proton luminosity to sub-Eddington levels. This can be understood as follows. First, the external photon energy, which typically lies in the optical/UV band, in the blob comoving frame appears (due to Doppler boosting) in the soft X-ray band, which is favorable for the production of sub-PeV/PeV neutrinos. Second, the photon number density in the jet’s comoving frame is enhanced, thus leading to higher neutrino production efficiency. However, given the high density of the Doppler-boosted external photon field, a strong magnetic field of $\sim 2 (u_{\text{BLR}}/\text{erg cm}^{-3})^{1/2} \text{ G}$ is required

to channel sufficient electron energy into synchrotron radiation and explain the low-energy bump of the SED. The produced synchrotron photons can still result in a high opacity for high-energy gamma rays (see Fig. 4), and then efficiently transfer energies of EM secondaries that are co-produced with neutrinos to the pair cascade. At the same time, the strong magnetic field enhances the synchrotron emission of the pair cascade in the X-ray band. Of course, one can adjust the model parameters to maximize the neutrino flux by reducing the magnetic field and the density of external photon field simultaneously. Nevertheless, on the premise of fitting the SED, a low neutrino detection rate similar to that in the one-zone SSC model is always obtained (Keivani et al. 2018).

3.3. Two-Zone $p\gamma$ model

In the two-zone $p\gamma$ model, the low-energy bump of the SED is produced by primary electrons in the outer blob, where the influence of the BLR radiation is negligible. Unlike the one-zone EC model, one does not have to adopt a strong magnetic field for the inner blob to explain the low-energy bump of the SED, as the latter is accounted for by the synchrotron radiation of primaries in the outer blob. The synchrotron radiation of primary electrons in the inner blob can be therefore suppressed by the EC process on the BLR radiation field, so that the $\gamma\gamma$ absorption for sub-PeV/PeV gamma rays is low. A large fraction of the energy injected into very high energy secondaries produced by the $p\gamma$ interactions will not be deposited in the EM cascade. Furthermore, secondary electrons generated in the cascades radiate mainly through the EC process. Hence, the X-ray flux from cascades is much lower than that in one-zone models, and subsequently allows for a much higher neutrino flux. Note that, the radiation field in the outer blob has little contribution to the absorption of gamma-rays escaping the inner blob (see Appendix B for details).

In Fig. 4, we compare the opacity of the $\gamma\gamma$ absorption in the inner blob as a function of the photon energy in the observer's frame for the two-zone $p\gamma$ model (with parameters given in Table 1), the one-zone SSC model with parameters from Cerruti et al. (2019)⁵, and the one-zone EC model with parameters from Keivani et al. (2018)⁶. The inner blob is optically thin to the attenuation of PeV photons in the two-zone model, but is predicted to be optically thick in the other two models,

⁵ i.e., $B = 0.2 \text{ G}$, $R = 1.5 \times 10^{16} \text{ cm}$, $\delta_D = 34$, $L_{e,\text{inj}} = 4 \times 10^{42} \text{ erg s}^{-1}$, $n_{e,1} = 2$, $\gamma_{e,\text{min}} = 500$, $\gamma_{e,\text{max}} = 1.5 \times 10^4$.

⁶ i.e., $B = 0.4 \text{ G}$, $R = 10^{17} \text{ cm}$, $\delta_D = 24.2$, $L_{e,\text{inj}} = 2.2 \times 10^{42} \text{ erg s}^{-1}$, $n_{e,1} = 1.9$, $n_{e,2} = 3.6$, $\gamma_{e,\text{min}} = 1$, $\gamma_{e,b} = 5 \times 10^3$, $\gamma_{e,\text{max}} = 8 \times 10^4$, $u_{\text{ext}} = 0.033 \text{ erg cm}^{-3}$.

as shown in Fig. 4.

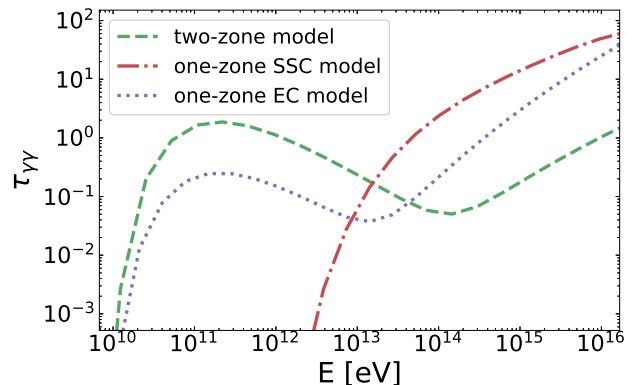


Figure 4. Comparison of the opacity of $\gamma\gamma$ annihilation as a function of the photon energy in the observer's frame in the two-zone $p\gamma$ model (dashed green curve), one zone EC model (dotted purple curve) and one-zone SSC model (dash-dotted red curve). See Section 3 for detailed discussion.

4. DISCUSSION AND CONCLUSIONS

4.1. Influence of the dusty torus

According to the unification scheme of AGN, a dusty torus (DT) is also expected to be present at large distances from the SMBH (i.e., $\sim 1 \text{ pc}$). Its radiation is treated as an isotropic blackbody spectrum with a peak at $3 \times 10^{13} \Gamma \text{ Hz}$ (Cleary et al. 2007) in the jet comoving frame. Denoting the DT luminosity by $L_{\text{DT}}^{\text{AGN}}$ in the AGN frame, the energy density of the DT radiation in the jet comoving frame varies with the distance to the SMBH ($r_{\text{in}}^{\text{AGN}}$), and it can be written as (Hayashida et al. 2012):

$$u_{\text{DT}} \approx \frac{\Gamma^2 L_{\text{DT}}^{\text{AGN}}}{4\pi (r_{\text{DT}}^{\text{AGN}})^2 c [1 + (r_{\text{in}}^{\text{AGN}}/r_{\text{DT}}^{\text{AGN}})^3]}, \quad (8)$$

where $r_{\text{DT}}^{\text{AGN}} = 2.5(L_{\text{DT}}^{\text{AGN}}/10^{45} \text{ erg s}^{-1})^{1/2} \text{ pc}$ is the characteristic radius of the DT in the AGN frame. This results in $r_{\text{DT}} \simeq 0.56 \text{ pc}$ assuming that $L_{\text{DT}}^{\text{AGN}} = L_{\text{BLR}}^{\text{AGN}}$ and the outer blob is not expected to be influenced by the DT radiation.

The typical energy of the DT radiation (as viewed in the jet's comoving frame) falls in optical band, thus acting as a target photon field for BH pair production and $\gamma\gamma$ pair production. As a result, inclusion of the DT in the radiative transfer calculations for the inner blob, leads to higher X-ray fluxes due to the injection of more sub-TeV/TeV electrons into the pair cascade.

On the other hand, the DT radiation field will suppress the synchrotron radiation of the sub-TeV/TeV electrons, which would produce X-ray emission. These two effects influence the X-ray emission from pair cascades in opposite directions and somewhat counteract

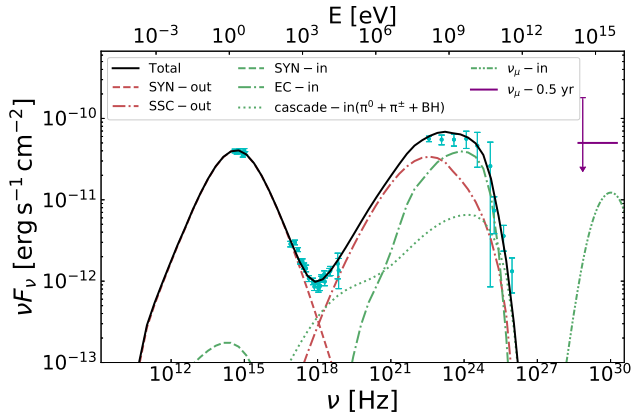


Figure 5. Same as in Fig. 3, except taking into account the presence of a dusty torus with luminosity 5×10^{43} erg/s. All other parameters are identical to those shown in Tab. 1.

each other. Indeed, from Fig. 5, we see that the maximal neutrino flux obtained (i.e., when the observed X-ray flux is saturated by the cascade emission) with inclusion of the DT radiation is comparable to that obtained previously in the absence of the DT (see e.g. Fig. 3). Therefore, whether a DT exists in this source or not has a minor influence on the SED fitting and neutrino flux.

4.2. Possible application to the 2014/2015 neutrino flare

The historical IceCube data in the position of TXS 0506+056 show a 3.5σ excess of high-energy muon neutrinos between September 2014 and March 2015, with 13 ± 5 events in the range of 32 TeV – 3.6 PeV (IceCube Collaboration et al. 2018b). This corresponds to an all-flavor isotropic-equivalent neutrino luminosity of $1.2_{-0.4}^{+0.6} \times 10^{47}$ erg s $^{-1}$. During this period, TXS 0506+056 was not exhibiting any flaring activity in electromagnetic radiation (from radio to gamma-rays), thus suggesting that the neutrino excess could not have been produced by an enhancement of the intensity of target radiation fields for the $p\gamma$ process. Thus, we can rule out the conventional one-zone model for the enhanced neutrino emission (Rodrigues et al. 2019; Wang et al. 2018b). Particularly, the isotropic-equivalent gamma-ray luminosity above 0.1 GeV is only one fifth of the neutrino luminosity. Such a feature has been interpreted as strong internal absorption of gamma-ray photons by X-ray radiation (Wang et al. 2018b; Reimer et al. 2018), which might arise from the thermalized radiation inside a massive cloud that enters the jet in the framework of two-zone pp model (Wang et al. 2018b). Here, we briefly discuss the potential of the two-zone $p\gamma$ model for explaining the 2014/2015 neutrino excess.

There are two basic observational constraints: (1) the blazar is not exhibiting any EM flare during the

neutrino excess, so there is no good physical reason for the proton injection luminosity to be super-Eddington; (2) unless one has an extremely large proton-to-electron ratio (i.e., baryon loading factor) for particle injection, the radiation of injected electrons needs to be suppressed or absorbed to avoid producing an EM flare. One possibility is to consider that the inner blob forms close to a hypothetical hot X-ray corona at a distance comparable to or a few times larger than the gravitational radius of the SMBH (i.e., $r_{\text{co}} \sim 10^{14} - 10^{15}$ cm). The corona’s radiation is thought to be produced by Compton upscattering of UV and optical photons from the SMBH accretion disk by hot electrons. It typically has a power-law spectrum with photon index $\alpha \simeq 1 - 2$ and a cutoff in the range of $\lesssim 100$ keV for AGN with high Eddington ratio (e.g., Kamraj et al. 2018; Ricci et al. 2018, though for non-blazar AGN). For simplicity, we neglect the effects of general relativity from the following qualitative discussion. Let us assume the corona’s luminosity to be $L_X = 10^{43}$ erg s $^{-1}$ at 1 keV which is comparable to that of the BLR. By using the Δ resonance approximation for the $p\gamma$ cross section, we find the production efficiency of neutrinos to be $f_\nu \simeq (3/8)\xi_\Delta\sigma_\Delta n_X r_{\text{co}} \sim 5 \times 10^{-3}(L_{X,1\text{keV}}/10^{43}\text{erg s}^{-1})(r_{\text{co}}/10^{14}\text{cm})^{-1}(E_\nu/15\text{TeV})^{\alpha-1}$, where $n_X = L_X/4\pi r_{\text{co}}^2 c \epsilon_X$ is the X-ray photon number density, $\xi_\Delta = 0.2$ is the inelastic coefficient of the $p\gamma$ interactions, the prefactor $3/8$ is the fraction of the energy lost by the proton that goes into neutrinos, and $\sigma_\Delta \simeq 4 \times 10^{-28}$ cm $^{-2}$ is the cross section of the Δ resonance. Assuming protons are injected with a differential kinetic luminosity $E_p^2 L_p^k(E_p) = 5 \times 10^{45}$ erg s $^{-1}$ (so that the proton’s kinetic luminosity integrated from 1 GeV to 100 PeV is still sub-Eddington), we obtain the all-flavor differential neutrino luminosity in the AGN frame as $E_\nu^2 L_\nu(E_\nu) = f_\nu(E_\nu) E_p^2 L_p^k(E_p = 20E_\nu) = 3 \times 10^{43}(E_\nu/15\text{TeV})^{\alpha-1}$ erg s $^{-1}$. Given a typical jet’s Doppler factor $\delta_D = 20$ and the corona’s spectral index $\alpha = 1$, the isotropic-equivalent neutrino luminosity in the range of 32 TeV – 3.6 PeV can be found by multiplying a factor of $\sim \delta_D^2 \ln(3600/32)$, resulting in $L_{\nu,\text{iso}} \sim 6 \times 10^{46}$ erg/s, which is consistent with the observation.

The synchrotron radiation of injected electrons are suppressed by the EC process on the X-ray radiation as long as the magnetic field in jet’s comoving frame is $\ll 10^4$ G (i.e., $U_B \ll U_{\text{co}}$). The IC radiation of electrons would produce GeV emission but the $\gamma\gamma$ opacity in the X-ray radiation field is $\tau_{\gamma\gamma} = \sigma_{\gamma\gamma} L_X/4\pi r_{\text{co}} c \epsilon_{X,1\text{keV}} \simeq 16(L_{X,1\text{keV}}/10^{43}\text{erg s}^{-1})(r_{\text{co}}/10^{14}\text{cm})^{-1}$. Such a large gamma-ray opacity is consistent with the fact that there is no associating gamma-ray flare with the neutrino flare. It is therefore possible to explain the EM and neutrino data of the 2014/2015 period within our model.

The absorbed GeV flux would be reprocessed into MeV band through the IC scattering on the external X-ray radiation field (Wang et al. 2018b; Inoue et al. 2019; Murase et al. 2019). During the 2014/2015 neutrino excess, there is no observation at MeV band that can constrain the model. Future MeV–GeV detectors such as e-ASTROGAM (de Angelis et al. 2018), AMEGO (Moiseev, & Amego Team 2017) and PANGU (Wu et al. 2016) would be able to test the model in a similar event.

4.3. The diffuse neutrino emission in the two-zone $p\gamma$ model

As we have shown in Section 2.4, the two-zone model can enhance the expected neutrino flux from TXS 0506+056. One may wonder how the predicted diffuse neutrino flux compares to the IceCube observations (Aartsen et al. 2017), if our model is generalized to the blazar population.

We here provide a rough estimate for the contribution of the blazar population to the diffuse neutrino flux in the context of the two-zone $p\gamma$ model. To do so, we simply use a scaling relation between the blazar gamma-ray luminosity and the expected neutrino luminosity, based on the results obtained in this work for the flaring state of TXS 0506+056. For simplicity, we do not exclude from our analysis the true BL Lac objects, which have no or weak BLR radiation, although their neutrino emission would also be weak. Therefore, the estimation of the diffuse neutrino flux in the two-zone model should be regarded as a crude upper limit.

According to the population study of GeV blazars by Ajello et al. (2014), the gamma-ray energy production rate of the entire population peaks at redshift $z \sim 1 - 2$ with a value of $\dot{W}_\gamma = 10^{46}$ erg Mpc $^{-3}$ yr $^{-1}$. For TXS 0506+056, the isotropic-equivalent gamma-ray flare luminosity is $\sim 10^{47}$ erg s $^{-1}$, and the muon neutrino luminosity at the spectral peak (i.e., PeV) predicted in the two-zone $p\gamma$ model is about 3×10^{45} erg s $^{-1}$. If we scale the PeV muon neutrino production rate with the gamma-ray production rate following the case of TXS 0506+056, we obtain a PeV muon neutrino production rate of $\dot{W}_\nu(\text{PeV}) = 1.5 \times 10^{43}(f_{\text{fl}}/0.05)$ erg Mpc $^{-3}$ yr $^{-1}$. Here f_{fl} is the duty factor of blazar flares (Murase et al. 2018), which is introduced by considering that the neutrino emission of blazar is dominated by the flare state. It then leads to a diffuse neutrino flux at PeV of

$$\begin{aligned} \Phi_\nu(1 \text{ PeV}) &\approx \frac{cf_{\text{fl}}\dot{W}_\nu(1 \text{ PeV})}{4\pi H_0} \\ &= 10^{-8} \left(\frac{f_{\text{fl}}}{0.05} \right) \text{GeV cm}^{-2}\text{s}^{-1}\text{sr}^{-1}. \end{aligned} \quad (9)$$

Note that the differential 90% C.L. upper limit

of diffuse muon neutrino flux from blazars is 10^{-8} GeVcm $^{-2}$ s $^{-1}$ sr $^{-1}$ at PeV (Aartsen et al. 2017). Therefore, our model is consistent with the observational constraints as long as the neutrino flare duty factor f_{fl} is $\lesssim 0.05$. Alternatively, even if the relevant flare duty factor is larger, the two-zone leptonic model is consistent with the observed upper limit of blazars to the IceCube neutrino flux, as long as only a fraction of gamma-ray flares in blazars are due to dissipation (i.e., particle acceleration) close to or inside the BLR where the neutrino production efficiency is high. Indeed, the BLR usually extends out to a distance of $\sim 0.1 - 1$ pc from the SMBH, and only a small fraction of the jet is close to or inside the BLR given a jet length of $10 - 100$ pc. If we assume dissipation or particle acceleration occur with an equal probability per unit length along the jet, the probability of forming a radiating zone inside the BLR should be $\sim 1 - 10\%$. Our argument may be supported by analysis of Costamante et al. (2018) who found that only 1 out of 10 FSRQs shows a feature of substantial attenuation in their gamma-ray spectrum, implying that only 10% of the emitting regions of FSRQs are close to or inside their BLRs.

4.4. Distinguishing between the two-zone $p\gamma$ model and other models

Liu et al. (2019) studied a two-zone pp model in which neutrinos are produced through pp collisions between accelerated protons and BLR clouds that enter the jet. This scenario is very similar to our two-zone $p\gamma$ model in terms of the physical separation of the regions responsible for the neutrino and low-energy photon emissions. Additionally, in the two-zone pp model, the BLR clouds that enter the jet will be fully ionized and, subsequently, the generated free electrons may further reduce the X-ray flux by deflecting X-ray photons into other direction from our line of sight via Compton scattering. As a result, the two-zone pp model is less constrained by the X-ray observations and can, in principle, lead to even higher neutrino flux than the one predicted in the two-zone $p\gamma$ model.

Both the pp and $p\gamma$ two-zone models can reproduce the SED of the blazar and generate a comparatively high neutrino flux. Yet, the predicted TeV neutrino spectrum can be used as a model diagnostic. The neutrino spectrum generated by pp collisions basically follows the spectrum of the parent protons, which is generally believed to be a power law extending down to GeV energies. On the contrary, the neutrino spectrum generated by $p\gamma$ interactions peaks around PeV energies and the flux drops quickly at lower energies because the number density of target photons needed to produce these low-energy neutrinos is too low. Thus, if the neutrino spectrum can be measured or constrained in the TeV–PeV

range in a blazar flare similar to that associated with IC-170922A in the future, we can distinguish between these two mechanisms. To achieve this goal, next-generation neutrino telescopes, such as IceCube-Gen2 with several times larger effective area compared to IceCube, are required.

Although the neutrino flux predicted by one-zone models for the 2017 flare of TXS 0506+056 is low, the model predictions are still consistent with the detection of one event. Despite the higher neutrino fluxes predicted in the framework of two-zone models, the expected number of muon neutrinos during the 2017 gamma-ray flare is still $\lesssim 1$. Thus, we cannot currently distinguish one-zone models from two-zone models for IC-170922A. However, if the same blazar flare was to occur in the era of IceCube-Gen2, the expected number of muon neutrinos in two-zone models would easily exceed unity, in contrast to one-zone models.

5. CONCLUSION

The neutrino event IC-170922A coincident with gamma-ray flare of blazar TXS 0506+056 has been explained as an upward fluctuation or as the first neutrino to be detected from an ensemble of faint neutrino emitting sources in one-zone models. In these models, the neutrino detection rate is strongly constrained by the X-ray observations, because X-ray emission is unavoidably produced by the synchrotron radiation of the secondary electrons developed in pair cascades accompanying the neutrino production.

In an attempt to obtain a higher neutrino detection rate than the one predicted with one-zone models, we proposed a two-zone $p\gamma$ model for the 2017 blazar flare. According to our scenario, two physically distinct emitting regions (blobs) are present in the blazar jet. In the inner blob, which is located inside or close to the BLR, relativistic electrons mainly radiate/cool via the EC process and neutrinos are efficiently produced via $p\gamma$ interactions of relativistic protons on Doppler-boosted BLR photons. In the outer blob, which is located well beyond the BLR, relativistic electrons radiate mainly via synchrotron and SSC processes; the neutrino production efficiency in this emitting region is low. We demonstrated that the combined emission from these two radiation zones can fit the SED of the blazar flare satisfactorily. We showed that the predicted PeV $\nu_\mu + \bar{\nu}_\mu$ flux during

the flare period can be as high as 10^{-11} erg cm $^{-2}$ s $^{-1}$, without invoking a super-Eddington luminosity for the injected protons.

Using the effective area of the IceCube EHE alert system, the predicted neutrino flux translates to a detection rate of ~ 0.3 yr $^{-1}$. The latter is about one order of magnitude larger than the one derived in one-zone models. The reason behind this difference is that the two-zone model relaxes the constraints imposed on the neutrino flux in two ways:

1. The emitting zone responsible for the low-energy hump of the SED is physically separated from the neutrino emitting region. As a result, the $\gamma\gamma$ absorption opacity for high-energy photons is significantly reduced in the neutrino emitting zone. This suppresses the emission from the EM cascade by reducing the number of high-energy photons/electrons that participate in the pair cascade.
2. In the presence of a dense external radiation field, the X-ray emission, which arises from the synchrotron radiation of electrons in the pair cascade, is suppressed by the EC process. As a result, the radiation of secondary pairs is channeled preferentially to higher energies than in X-rays.

Currently, it is difficult to discriminate the two-zone $p\gamma$ model presented here from other scenarios proposed for the multi-messenger flare of TXS 0506+056. This may become possible with future high-energy neutrino detections from TXS 0506+056 or other blazars by next-generation neutrino telescopes with larger effective areas, such as IceCube-Gen2.

This work is supported by the National Key R&D program of China under the grant 2018YFA0404200, and the NSFC under grants 11625312 and 11851304. F.O. is supported by the Deutsche Forschungsgemeinschaft through grant SFB1258 “Neutrinos and Dark Matter in Astro- and Particle Physics”. M.P. acknowledges support from the Lyman Jr. Spitzer Postdoctoral Fellowship and NASA Fermi 80NSSC18K1745. K.W. is supported by the China Postdoc Science Grant (No. 2019M650311).

APPENDIX

A. EXPLAINING THE SED WITH OTHER SET OF PARAMETERS

In our default SED fit shown in Fig. 3, we assumed the same magnetic field strength and injection electron spectrum for both blobs, despite their large separation, with the only requirement that $R_{\text{out}} \gtrsim R_{\text{in}}$. Our assumption implies that either the jet is not conical or that the size of the outer blob is much smaller than the jet’s transverse radius at that location. The latter scenario has been also proposed to explain the fast variability of the optical blazar emission,

Table A1. Model parameters for SED fit shown in the left panel of Fig. A1

Free parameters	δ_D	B	R_{out}	R_{in}	$L_{\text{e,inj}}$	$r_{\text{out}}^{\text{AGN}}$	$r_{\text{in}}^{\text{AGN}}$	$n_{\text{e},1}$	$n_{\text{e},2}$	$\gamma_{\text{e,b}}$
		[G]	[cm]	[cm]	[erg/s]	[pc]	[pc]			
Values	26.5	0.12	8×10^{16}	2×10^{16}	1.7×10^{42}	10	0.07	2	4	1×10^4
Fixed/Derived parameters	$L_{\text{BLR}}^{\text{AGN}}$	$L_{\text{p,inj}}$	$\gamma_{\text{e,min}}$	$\gamma_{\text{e,max}}$	n_{p}	$\gamma_{\text{p,min}}$	$\gamma_{\text{p,max}}$	$L_{\text{e,in}}^k$	$L_{\text{p,in}}^k$	
	[erg/s]	[erg/s]						[erg/s]	[erg/s]	
Values	5×10^{43}	1.97×10^{44}	50	10^7	2	1	1.09×10^7	1.02×10^{44}	1.3×10^{47}	

if this is emitted at a large distance from the SMBH (Tavecchio et al. 2011).

Our default SED fit shown in Fig. 3 is not unique. In fact, because of the multi-parameter nature of two-zone models, it is often not possible to constrain their free parameters by SED fitting alone. For the purposes of this work, it is sufficient to find a set of reasonable parameters for fitting the SED and demonstrate the feasibility of the model. Nevertheless, it is useful to discuss different parameter combinations that can still describe well the SED and, at the same time, correspond to different physical realizations. In the following, we consider two alternative scenarios.

Let us first look into a case where the GeV flux is dominated by the EC emission from the inner blob. To achieve this, we simply suppress the SSC emission of the outer blob by adopting a few times larger radius than the one used in our default fit (see Tables 1 and A1). For the adopted parameters, the SSC flux from the outer blob is comparable to the gamma-ray flux in the *Fermi*-LAT band at a low state. If there is no dissipation happening close to the BLR (i.e., without the inner blob), the outer blob can solely explain the SED in the low state, without expecting significant neutrino emission. Note that electrons cool quite fast in the inner blob (under the parameters in Table A1, a cooling break will appear in the electron spectrum at $\gamma_{\text{cool}} \approx 75$), so the spectral index of the steady-state electrons responsible for GeV emission is $n_{\text{e},1} + 1$ and thus we assume $n_{\text{e},1} = 2$ to account for the flat spectrum observed at GeV. The results are shown in the left panel of Fig. A1.

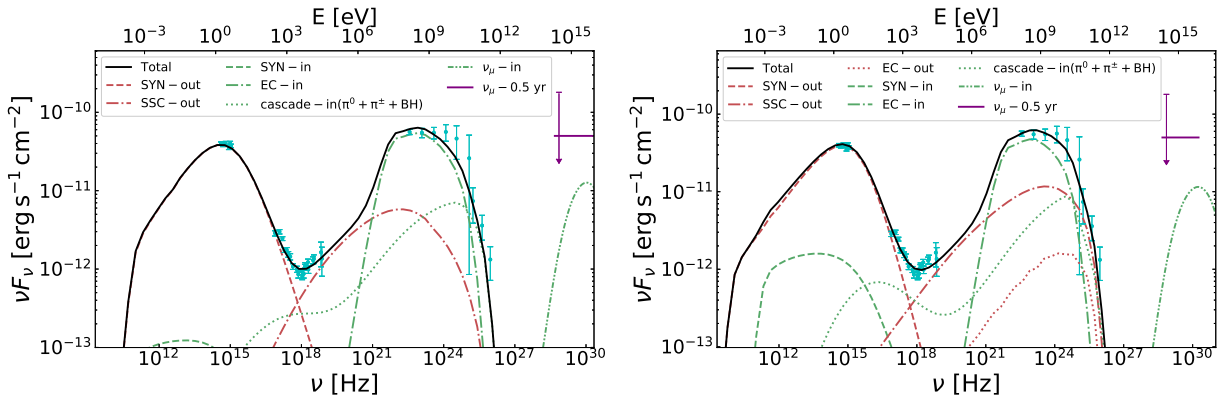


Figure A1. Examples of SED fits obtained within the context of our two-zone model for different parameter sets. In both cases, the GeV gamma-ray flux is dominated by the EC emission from the inner blob, unlike the default SED fit shown in Fig. 3. In the right panel, the magnetic field and the blob radius are scaled to the distance of the blob from the SMBH. The line styles have the same meaning as in Fig. 3. The parameter values used for the models shown in the left and right panels are summarized in Tables A1 and A2, respectively.

We next consider a case where the blob radius is related to the blob distance from the SMBH. In particular, we assume that both blobs occupy the entire cross section of a conical jet, with R_{out} and R_{in} following the relation $R_{\text{out}}/r_{\text{out}} = R_{\text{in}}/r_{\text{in}}$. We also consider that the blob magnetic field strength decreases along the jet in the same way as the poloidal component of the jet's magnetic field in magnetohydrodynamical models (i.e., $B \propto r^{-1}$) (e.g., Vlahakis 2004; Komissarov et al. 2007; O'Sullivan, & Gabuzda 2009; Zamaninasab et al. 2014; Yan et al. 2018). In addition, we relax the assumption of the same particle injection spectrum for the two blobs. The fitting result is shown in the right panel of Fig. A1 and the free parameters are listed in Table A2.

Table A2. Model parameters for the SED fit shown in the right panel of Fig. A1.

Free parameters	δ_D	B_{in}	R_{in}	$L_{e,\text{inj},\text{in}}$	$r_{\text{in}}^{\text{AGN}}$	$n_{e,1,\text{in}}$	$n_{e,2,\text{in}}$	$\gamma_{e,b,\text{in}}$		
		B_{out}	R_{out}	$L_{e,\text{inj},\text{out}}$	$r_{\text{out}}^{\text{AGN}}$	$n_{e,1,\text{out}}$	$n_{e,2,\text{out}}$	$\gamma_{e,b,\text{out}}$		
		[G]	[cm]	[erg/s]	[pc]					
Values	26.5	0.37	2×10^{16}	1.12×10^{42}	0.08	2	3.8	1×10^4		
		0.006	1.25×10^{18}	5.7×10^{43}	5	2.2	4.5	5.93×10^4		
Fixed/Derived parameters	$L_{\text{BLR}}^{\text{AGN}}$	$L_{p,\text{inj}}$	$\gamma_{e,\text{min}}$	$\gamma_{e,\text{max}}$	n_p	$\gamma_{p,\text{min}}$	$\gamma_{p,\text{max}}$	$L_{e,\text{in}}^k$	$L_{p,\text{in}}^k$	
	[erg/s]	[erg/s]						[erg/s]	[erg/s]	
Values	5×10^{43}	1.97×10^{44}	50	10^7	2	1	4.74×10^7	1.24×10^{44}	1.3×10^{47}	

B. CONTRIBUTION OF THE OUTER BLOB'S RADIATION TO THE OPACITY OF GAMMA-RAY PHOTONS EMITTED BY THE INNER BLOB

In the SED fitting in the main text (Fig. 3), we employ $\delta_D = \Gamma = 26.5$ which corresponds to a viewing angle of about 2 degree with respect to the jet's axis. In other word, we can observe photons/neutrinos which are emitted into this specific direction (in the AGN frame). The gamma-ray photons emitted from the inner blob may encounter the photon radiated by the outer blob and might be absorbed via $\gamma\gamma$ annihilation. Let us calculate the opacity of this process in the jet comoving frame and hereafter we denote quantities in jet's comoving frame with primes. Since we consider blobs as stationary features (see Section 2.4 in the jet, the distance between the two blobs in the jet's comoving frame becomes d/δ_D). According to the Lorentz transform of the cosine of an angle, a photon that is emitted towards observer's direction has an angle $\theta' \sim 90$ degree with respect to the jet axis in the jet's comoving frame (i.e., $\mu' = (\mu - \beta)/(1 - \mu\beta)$, where $\mu = \cos\theta$ and $\mu' = \cos\theta'$, β is the jet velocity in unit of c). Noting that the outer blob's emission is isotropic in the jet's comoving frame and regarding the outer blob as a point source, we can integrate over the path of the gamma-ray photon to get the opacity with a delta-function approximation for the cross section of $\gamma\gamma$ annihilation, i.e.,

$$\tau_{\gamma\gamma} = \int_0^\infty \frac{\sigma_{\gamma\gamma}(1 - \cos\alpha')L_{\text{syn}}/\delta_D^4}{4\pi[(d/\delta_D)^2 + x'^2]c(\epsilon_{\text{opt}}/\delta_D)} dx' = \frac{\sigma_{\gamma\gamma}L_{\text{syn}}}{4\pi d\delta_D^2 c\epsilon_{\text{syn}}} \int_0^\infty \frac{1 - y/(1 + y^2)^{1/2}}{1 + y^2} dy = \frac{(\pi/2 - 1)\sigma_{\gamma\gamma}L_{\text{syn}}}{4\pi d\delta_D^2 c\epsilon_{\text{syn}}}, \quad (\text{B1})$$

where $y \equiv x'\delta_D/d$ with x' denoting the distance travelled by the high-energy photon in the jet's comoving frame. $\cos\alpha' = x'/[x'^2 + (d/\delta_D)^2]^{1/2}$ is the cosine of the collision angle between the gamma-ray photon and the soft photon from the outer blob, L_{syn} is the isotropic-equivalent luminosity of synchrotron radiation of the outer blob and ϵ_{syn} is the peak energy of the synchrotron radiation (in AGN frame). We are concerned with the opacity for high-energy photons co-produced with neutrinos (e.g., 1PeV photons), thus we look for parameters of soft photon at $\epsilon_{\text{syn}} = 10^{12} \text{ eV}^2 \delta_D^2 / 10^{15} \text{ eV} = 0.7 \text{ eV}$, where $L_{\text{syn}} = 10^{46} \text{ erg/s}$ is employed. For $d = 10 \text{ pc}$, we have $\tau_{\gamma\gamma}(1\text{PeV}) = 0.06$ which can be neglected. We verify the above analysis in Fig. B3 by calculating the opacity numerically with the synchrotron radiation spectrum obtained in Fig. 3 and the full cross section of $\gamma\gamma$ annihilation (Aharonian et al. 1983). We can see that the numerical result at 1PeV is only a factor of 2 larger than the analytical estimation when integrating x' up to 100 pc, which is still smaller than unity for photon of energy $<10\text{PeV}$. We also show the result with integrating x' up to 0.1 pc for comparison. Therefore, we conclude that the radiation from the outer blob has little influence on the gamma-ray photons emitted by the inner blob in our model (at least with the employed parameters).

REFERENCES

- Aartsen, M. G., Abraham, K., Ackermann, M., et al. 2017, ApJ, 835, 45
- Abdo, A. A., Ackermann, M., Agudo, I., et al. 2010, ApJ, 716, 30
- Aharonian, F. A., Atoian, A. M., & Nagapetian, A. M. 1983, *Astrofizika*, 19, 323
- Ajello, M., Romani, R. W., Gasparrini, D., et al. 2014, ApJ, 780, 73
- Alvarez-Muñiz, J., & Mészáros, P. 2004, Physical Review D, 70, 123001
- Ansoldi, S., et al. 2018, ApJL, 862, L10
- Atoyan, A., & Dermer, C. D. 2001, PhRvL, 87, 221102
- Atoyan, A. M., & Dermer, C. D. 2003, ApJ, 586, 79
- Bednarek, W. & Protheroe, R. J. 1999, MNRAS, 302, 373
- Böttcher, M., Reimer, A., Sweeney, K., & Prakash, A. 2013, ApJ, 768, 54
- Celotti, A., & Ghisellini, G. 2008, MNRAS, 385, 283
- Cerruti, M., Zech, A., Boisson, C., et al. 2019, MNRAS, 483, L12
- Chodorowski, M. J., Zdziarski, A. A., & Sikora, M. 1992, ApJ, 400, 181
- Cleary, K., Lawrence, C. R., Marshall, J. A., Hao, L., & Meier, D. 2007, ApJ, 660, 117
- Costamante, L., Cutini, S., Tosti, G., et al. 2018, MNRAS, 477, 4749
- Dermer, C. D., Murase, K., & Takami, H. 2012, ApJ, 755, 147

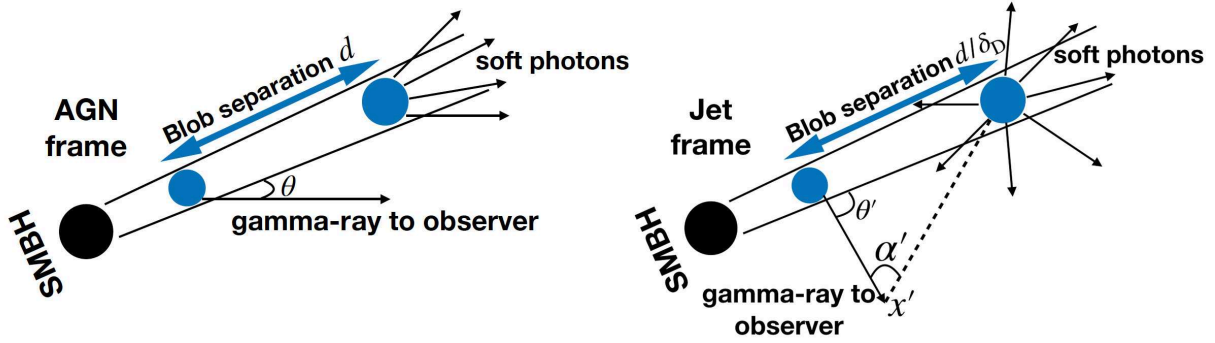


Figure B2. A sketch, not to scale, of the radiation direction in different reference frames. The left and the right panel shows the geometry in the AGN frame and the jet’s comoving frame respectively. A high-energy photon that propagates towards the observer moves at an angle θ' with respect to the jet’s axis. The high-energy photon collides with a low-energy photon from the outer blob at a distance of x' from the inner blob with a collision angle α' . See Appendix B for more discussion.

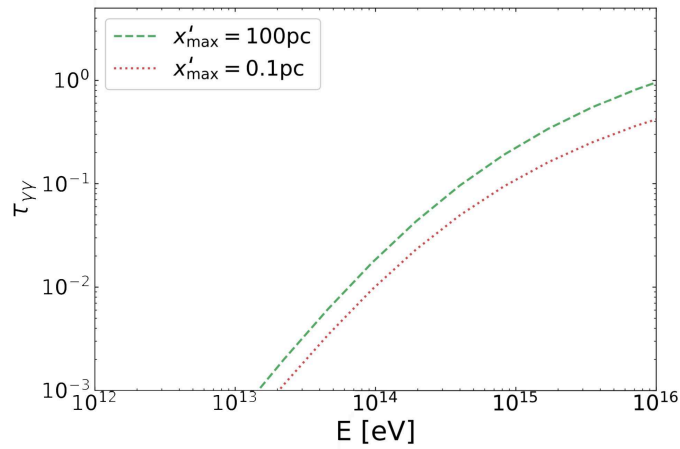


Figure B3. $\gamma\gamma$ absorption opacity due to the radiation of the outer blob for high-energy photons emitted from the inner blob. The horizontal axis is the gamma-ray energy in the AGN frame. The dashed green curve and the dotted red curve show the opacity after high-energy photons having travelled a distance of 100 pc and 0.1 pc, respectively, in the comoving frame.

- Dermer, C. D., Murase, K., & Inoue, Y. 2014, *Journal of High Energy Astrophysics*, 3, 29
- de Angelis, A., Tatischeff, V., Grenier, I. A., et al. 2018, *Journal of High Energy Astrophysics*, 19, 1
- Domínguez, A., Primack, J. R., Rosario, D. J., et al. 2011, *MNRAS*, 410, 2556
- Fromm, C. M., Perucho, M., Ros, E., et al. 2011, *A&A*, 531, A95
- Gao, S., Fedynitch, A., Winter, W., & Pohl, M. 2019, *Nature Astronomy*, 3, 88
- Georganopoulos, M., & Marscher, A. P. 1998, *ApJ*, 506, 621
- Ghisellini, G., Tavecchio, F., Foschini, L., et al. 2010, *MNRAS*, 402, 497
- Giommi, P., Padovani, P., Polenta, G., et al. 2012, *MNRAS*, 420, 2899
- Giommi, P., Padovani, P., & Polenta, G. 2013, *MNRAS*, 431, 1914
- Harris, D. E., & Krawczynski, H. 2006, *ARA&A*, 44, 463
- Hayashida, M., Madejski, G. M., Nalewajko, K., et al. 2012, *ApJ*, 754, 114
- IceCube Collaboration, Aartsen, M. G., Ackermann, M., et al. 2018, *Science*, 361, eaat1378
- IceCube Collaboration, Aartsen, M. G., Ackermann, M., et al. 2018, *Science*, 361, 147
- Inoue, Y., Khangulyan, D., Inoue, S., et al. 2019, *The Astrophysical Journal*, 880, 40
- Kamraj, N., Harrison, F. A., Baloković, M., et al. 2018, *ApJ*, 866, 124
- Katarzyński, K., Sol, H., & Kus, A. 2001, *A&A*, 367, 809
- Kimura, S. S., Murase, K., & Toma, K. 2015, *The Astrophysical Journal*, 806, 159
- Keivani, A., Murase, K., Petropoulou, M., et al. 2018, *ApJ*, 864, 84
- Kelner, S. R., & Aharonian, F. A. 2008, *PhRvD*, 78, 034013
- Komissarov, S. S., et al. 2007, *MNRAS*, 380, 1
- Lagage, P. O., & Cesarsky, C. J. 1983, *A&A*, 125, 249
- Liu, R.-Y., Wang, K., Xue, R., et al. 2019, *PhRvD*, 99, 063008
- Madejski, G. M., Nalewajko, K., Madsen, K. K., et al. 2016, *ApJ*, 831, 142
- Mannheim, K., & Biermann, P. L. 1992, *A&A*, 253, L21
- Mannheim, K., Stanev, T., & Biermann, P. L. 1992, *A&A*, 260, L1
- Mastichiadis, A., & Kirk, J. G., 1997, *A&A*, 320
- Moderski, R., Sikora, M., Coppi, P. S., & Aharonian, F. 2005, *MNRAS*, 363, 954
- Moiseev, A., & Amego Team 2017, 35th International Cosmic Ray Conference (ICRC2017), 798
- Murase, K., Inoue, Y., & Dermer, C. D. 2014, *PhRvD*, 90, 23007
- Murase, K., Guetta, D., & Ahlers, M. 2016, *Physical Review Letters*, 116, 071101
- Murase, K., Oikonomou, F., & Petropoulou, M. 2018, *ApJ*, 865, 124

- Murase, K., Kimura, S. S., & Meszaros, P. 2019, arXiv e-prints, arXiv:1904.04226
- Nalewajko, K., Sikora, M., Madejski, G. M., et al. 2012, *ApJ*, 760, 69
- O'Sullivan, S. P., & Gabuzda, D. C. 2009, *MNRAS*, 400, 26
- Padovani, P., Resconi, E., Giommi, P., Arsioli, B., & Chang, Y. L. 2016, *MNRAS*, 457, 3582
- Padovani, P., Oikonomou, F., Petropoulou, M., Giommi, P., & Resconi, E. 2019, *MNRAS*, 484, L104
- Paiano S., Falomo R., Treves A., & Scarpa R. 2018, *ApJL*, 854, L3
- Palladino, A., Rodrigues, X., Gao, S., & Winter, W. 2019, *ApJ*, 871, 41
- Plavin, A. V., Kovalev, Y. Y., & Petrov, L. Y. 2019, *ApJ*, 871, 143
- Petropoulou, M., Dimitrakoudis, S., Padovani, P., Mastichiadis, A., & Resconi, E. 2015, *MNRAS*, 448, 2412
- Petropoulou, M., & Mastichiadis, A. 2015, *MNRAS*, 447, 36
- Petropoulou, M., Coenders, S., Vasilopoulos, G., Kamble, A., & Sironi, L. 2017, *MNRAS*, 470, 1881
- Prince, R., Gupta, N., & Nalewajko, K. 2019, arXiv e-prints, arXiv:1908.04803
- Protheroe, R. J., & Clay, R. W. 2004, *PASA*, 21, 1
- Reimer, A., Boettcher, M., & Buson, S. 2018, arXiv e-prints, arXiv:1812.05654
- Rieger, F. M., Bosch-Ramon, V., & Duffy, P. 2007, *Ap&SS*, 309, 119
- Ricci, C., Ho, L. C., Fabian, A. C., et al. 2018, *MNRAS*, 480, 1819
- Righi, C., Tavecchio, F., & Inoue, S. 2019, *MNRAS*, 483, L127
- Rodrigues, X., Gao, S., Fedynitch, A., et al. 2019, *ApJL*, 874, L29
- Sahakyan, N. 2018, *ApJ*, 866, 109
- Stecker, F. W., Done, C., Salamon, M. H., et al. 1991, *Physical Review Letters*, 66, 2697
- Stickel M. et al. 1991, *ApJ*, 374, 431
- Stoeke J. T. et al. 1991, *ApJS*, 76, 8
- Strotjohann, N. L., Kowalski, M., & Franckowiak, A. 2019, *A&A*, 622, L9
- Tavecchio, F., & Ghisellini, G. 2008, *MNRAS*, 386, 945
- Tavecchio, F., Becerra-Gonzalez, J., Ghisellini, G., et al. 2011, *A&A*, 534, A86
- Tavecchio, F., Ghisellini, G., & Guetta, D. 2014, *The Astrophysical Journal*, 793, L18
- Tavecchio, F., & Ghisellini, G. 2015, *MNRAS*, 451, 1502
- Urry, C. M., & Padovani, P. 1995, *PASP*, 107, 803
- Vlahakis, N. 2004, *Ap&SS*, 293, 67
- Wang, K., Liu, R.-Y., Dai, Z.-G., & Asano, K. 2018, *ApJ*, 857, 24
- Wang, K., Liu, R.-Y., Li, Z., et al. 2018, arXiv e-prints, arXiv:1809.00601
- Wu, X., Walter, R., Su, M., et al. 2016, *Proc. SPIE*, 99056E
- Xue, R., Liu, R.-Y., Wang, X.-Y., Yan, H., & Böttcher, M. 2019, *ApJ*, 871, 81
- Yan, D., & Zhang, L. 2015, *MNRAS*, 447, 2810
- Yan, D., Wu, Q., Fan, X., et al. 2018, *ApJ*, 859, 168
- Zamaninasab, M., Clausen-Brown, E., Savolainen, T., et al. 2014, *Nature*, 510, 126
- Zhang, H., Fang, K., Li, H., et al. 2019, *ApJ*, 876, 109